Three-Dimensional Reconstruction of the Bony Structures involved in the Articular Complex of the Human Shoulder Using Shape-Based Interpolation and Contour-Based Extrapolation

Alexandra Branzan Albu, Denis Laurendeau
Computer Vision and Systems Laboratory, Dept. of Electrical Engineering, Laval University, Québec (QC) G1K 7P4, Canada
branzan@gel.ulaval.ca
laurend@gel.ulaval.ca

Luc J. Hébert
National Defence of Canada, Health Services Delivery, CS Valcartier succ FORCES Courcelette (QC) GOA 4Z0
ljhebert@videotron.ca

Hélène Moffet
Dept. of Readaptation, Faculty of Medecine, Laval University, Québec (QC) G1K 7P4

Christian Moisan
iMRI Unit, Québec City University Hospital, Québec (Qc) G1L 3L5, Canada
christian.moisan@rad.ulaval.ca

Abstract

In this paper, we propose a 3D reconstruction approach using shape-based interpolation and contour-based extrapolation. This approach aims to generate a 3D geometric model of a human shoulder from a sequence of MR parallel 2D cross-sections.
While interpolation generates intermediate slices between every pair of adjacent input slices, extrapolation performs a smooth closing of the external surface of the model. We propose a new interpolation method based on conditional morphological dilation. Our extrapolation approach is based on surface smoothness constraints and gradually shrinks every extreme 2D cross-section of a bony structure towards a point, respectively. Surface rendering is accomplished through the generation of a triangular mesh using a parametric representation of 2D slice contours. After surface rendering, local surface irregularities are smoothed with Taubin's surface fairing algorithm[11].

1. Introduction

Widely used medical imaging systems based on MR, X-rays, positron-emission, or ultrasound, scan 3D anatomic structures in a serial sequence of 2D parallel image slices. In order to visualize, analyze, and manipulate this data, one has to deal with the difference between the inter- and intra-slice resolution. The intra-slice resolution is usually much higher than the inter-slice resolution due to technical limitations and /or to medical reasons (i.e. respiratory motion artefact, limited interval of exposure to radiation). This is the reason why interpolation and/or extrapolation techniques are required to reconstruct the missing slices.

While a wide variety of interpolation methods are available in the medical imaging literature, extrapolation techniques are rarely proposed, mostly because of the difficulty in validating the results.

Interpolation techniques can be classified in two main categories with respect to their input information : grey-level and shape-based. Hybrid strategies have also been developed lately. Traditional grey-level interpolation techniques like the nearest neighbour method [1], linear grey-level interpolation [1],[2], higher order polynomial interpolation, and cubic spline interpolation [3] consist in the direct computation of intensity for every pixel in the interpolated slice. For medical imaging applications which are strongly object-oriented, grey-level interpolation techniques are not very suitable, since they result in a large amount of input data for further segmentation and in errors occurring in segmentation due to prior interpolation [4]. Shape-based interpolation techniques have been shown in [5] to be more efficient than grey-level interpolation methods. Shape-based interpolation techniques are object-oriented and aim at interpolating the binary object cross-section, rather than the grey-scale values. Since segmentation is performed before shape-based interpolation in most medical applications, the non–trivial task of segmenting intermediate slices is eliminated.

One of the first shape-based interpolation techniques, marking the conceptual transition from grey-level to shape-based approaches, is proposed in [4]. The binary images are converted into grey-level images by considering the distance transform and a grey-level interpolation is performed afterwards. A 3D reconstruction technique using a linear approach for shape-based interpolation and extrapolation is presented in [6].

Mathematical morphology offers a coherent framework for developing effective shape-based interpolation algorithms [7]. In [8], an interpolation technique based on morphological skeleton matching is proposed. The sensitivity of the morphological skeleton to noise is significantly reduced by using generalized fuzzy

mathematical operators in [9]. The morphological morphing transform proposed in [10] interpolates a new group of slices between each two consecutive image slices by performing a gradual shape transition. Our proposed scheme is similar to this approach. However, the morphing approach in [10] performs iterative erosions of the boundary elements in the initial set corresponding to the background of the final set. We observed that, in the case of a non-convex initial shape, iterative erosions may divide the foreground in disjoint regions, thus obstructing a smooth shape transition. Instead, we propose a morphing technique based on conditional dilation. Whereas in [10], the inter-slice resolution in the interpolated 3D object is non-uniform due to variable-length morphing sequences between different pairs of consecutive slices, we are able to obtain a 3D model with an uniform and adjustable inter-slice resolution. To be able to adjust the inter-slice resolution, we associate a coefficient of redundancy based on a shape similarity measure to every intermediate object in a "morphing" sequence.

In this paper, we propose a 3D reconstruction approach using shape-based interpolation and extrapolation. We propose a new interpolation approach based on *morphological morphing and "splitting"* that insures a smooth transition between every two adjacent input shapes. After interpolation, a *closing surface* step is performed using a new contour-based extrapolation technique. The 3D reconstructed model integrates the "closing" and "morphing" sequences in a coherent manner, allowing an adjustable uniform inter-slice resolution. Figure 1 shows the diagram of the proposed 3-D reconstruction algorithm.

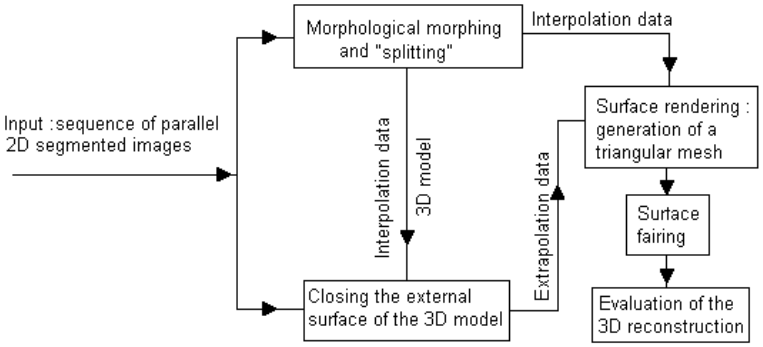

Figure 1. The diagram of the proposed 3D reconstruction algorithm

We use the proposed approach for reconstructing the bony structures involved in the articular complex of the human shoulder. The 3D reconstructed shoulder models allow for the study of the subacromial space in patients with shoulder impingement syndrome.

The organization of this paper is as follows. Section 2 presents our original 3D reconstruction approach. Section 3 presents and validates the approach with experimental results, while section 4 draws the conclusions and describes future work.

2. Reconstruction approach

For each patient, a serial sequence of 2D MR images of saggital shoulder slices is provided. Prior to the 3D reconstruction every image in the sequence was segmented with an algorithm based on isolabel contours [12].

In any input cross-section, the foreground contains one or more compact and disjoint regions corresponding to the scanned bony structures. Since bones exhibit a smoothly changing appearance from one slice to the next, no shape alignment is necessary prior to interpolation.

The following sub-sections present the main steps of the 3D reconstruction process.

2.1. Morphing-based interpolation

2.1.1. Mathematical background

Mathematical morphology [7] considers 2D binary images as sets of pixels on which set operations such as translation, union and intersection can be performed. The *dilation* of set A using the structuring element K is defined as :

$$A \oplus K = \bigcup \{A_k \,|\, k \in K\} \qquad (1)$$

where : $\oplus$ stands for the dilation operator; A_k is the translated set A, centered at an element k in K; K is the cross-shaped structuring element derived from the 4-connectivity neighbourhood.

We define a new morphological operator, *the conditional dilation* as follows.

Definition : Let A and B be two sets, with $B \subset A$. The *conditional dilation* of set B using structuring element K and with respect to reference set A is defined as :

$$B \oplus K\big|_A = \left(\bigcup \{B_k \,|\, k \in K\}\right) \cap A \qquad (2)$$

It can be easily proven that a finite number m of successive conditional dilations is required to generate A from B, that is :

$$\left(B \oplus K\big|_A\right)^m = A \qquad (3)$$

2.1.2 Morphological morphing of two simple compact regions

The morphing technique presented in this section generates a gradual transition between two compact and partially overlapping shapes. As input data for the proposed morphological morphing approach, we consider two binary compact regions located in adjacent slices and denoted by obj_1 and obj_2 respectively. These regions must correspond to the same bony structure, therefore they must be compact (with no interior holes) and partially overlapping when viewed in the normal direction to the slice plane. The result of the morphing technique is an *elementary morphing sequence* of intermediate binary objects gradually changing their shape from obj_1 towards obj_2.

In order to gradually transform obj_1 into obj_2 we perform two parallel deformation processes based on iterative conditional dilation. Given obj_0, the intersection between obj_1 and obj_2, the two deformation processes transform obj_0 into obj_1 and into obj_2 using k_1 and k_2 iterations respectively. Let $obj_{01}(i)$ and $obj_{02}(i)$ be the objects generated after i conditional dilations of obj_0 with respect to obj_1 ($i<k_1$) and, obj_2 ($i<k_2$) respectively. The morphing process transforms obj_1 into obj_2 by generating an *elementary morphing sequence* obj_{12} as follows :

$$obj_{12}(i) = \begin{cases} obj_{01}(k_1 - i) \cup obj_{02}(i) & \text{if } i < k_1 \le k_2 \\ & \text{or } i < k_2 \le k_1 \\ obj_{02}(i) & \text{if } k_1 \le i \le k_2 \\ obj_{01}(k_1 - i) \cup obj_{02}(k_2) & \text{if } k_2 \le i \le k_1 \end{cases} \qquad (4)$$

i = 1..max(k_1, k_2).

Figure 2 illustrates the morphing process between two synthetic objects, obj_1 (see fig. 2a) and obj_2 (see fig. 2g) respectively.

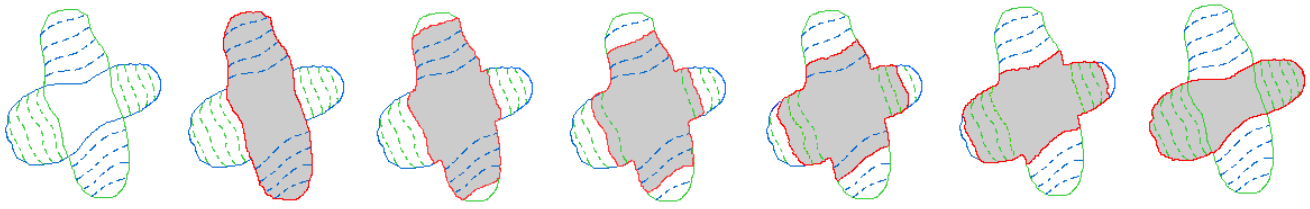

Figure 2. Morphing based on conditional dilation : a) superposition of the initial shape obj_1(green boundary) and the final shape obj_2 (blue boundary); the iterative conditional dilations of obj_0 with respect to obj_1 and of obj_2 are in dashed lines; b)initial shape (obj_1); c), d), e), f) intermediate iterations in the morphing process : intermediate objects are grey with red boundaries; g) final shape(obj_2)

The length of the elementary morphing sequence is equal to max(k_1, k_2) and thus it depends on how different the input shapes obj_1 and obj_2 located in adjacent slices are. However, in order to reconstruct a 3D model with uniform inter-slice resolution, the interpolation process is to generate the same number of intermediate slices between any two adjacent input slices, thus there is an *equal-length constraint* for *elementary interpolation sequences*. An fixed-length *elementary interpolation sequence* is defined as the result of interpolation for two adjacent input slices, and is obtained from *an elementary morphing sequence* by eliminating *"redundant"* intermediate objects. An intermediate object is considered *"redundant"* if it does not present a significant change of shape with respect to the previous or to the next object in the sequence. In order to avoid drastic shape changes in the elementary interpolation sequence, elimination is an iterative process, and the most "redundant" object is eliminated at the current iteration.

To evaluate the "redundancy" of intermediate objects, a *shape distance measure* is defined as follows :

$$d(obj(i), obj(i+1)) = card(obj\ (i) \,\Delta\, obj(i+1)) \qquad (5)$$

where $obj(i)$ and $obj(i+1)$ are successive intermediate slices in the elementary morphing sequence and Δ stands for the symmetric difference. At every iteration k of the elimination process a set of *redundancy coefficients* corresponding to the intermediate objects in the current sequence is computed as follows :

$$\rho(obj(i)) = min\left(d(obj(i), obj(i-1))^{-1}, d(obj(i), obj(i+1))^{-1}\right) \qquad (6)$$

i = 2..($L(k)$-1), where $L(k)$ is the length of the sequence at iteration k. The first and the last objects in an elementary morphing sequence are not eliminated, since they represent input slices in the reconstruction process. The object with the highest redundancy coefficient is eliminated at the current iteration, and the resulting sequence represents the input for the next iteration. The redundancy coefficients are updated at every iteration. The elimination process stops when the length of the

sequence becomes equal to the fixed length for the elementary input sequence.

The equal-length constraint for elementary interpolation sequences results in an uniform inter-slice resolution of the 3D reconstructed model. Furthermore, we use the method of redundancy coefficients for varying the length of the elementary morphing sequences. Thus, we are able to generate 3D models of variable size and adjustable inter-slice resolution.

2.1.3. A morphological "splitting" approach

Since anatomic structures have a continuous appearance, the inter-slice region correspondence problem has a straightforward solution, which maximizes the following maximum inter-slice region overlap criterion :

$$C(R_i, R'_{i+1}) = \begin{cases} 1 \text{ if } card(R_i \cap R'_{i+1}) = max \\ 0 \qquad\qquad \text{otherwise} \end{cases} \qquad (7)$$

where R_i , R'_{i+1} are compact regions in adjacent slices i and i+1 respectively.

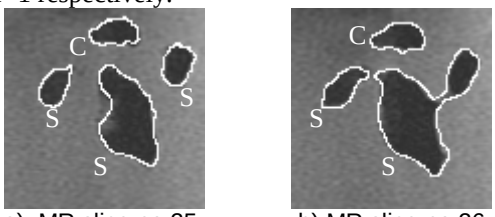

a) MR slice no.25 b) MR slice no.26

Figure 3. A "branching" case in a human shoulder MR sequence : a) three disjoint scapula(S) regions; b) merging of the previous right-most two scapula regions into one region. S-scapula; C-clavicle;

A "branching" situation as shown in Figure 3 occurs when two disjoint regions in slice i(or i+1) correspond to the same compact region in slice i+1(or i respectively). We give a particular attention to the "branching" problem, since it has important repercussions on interpolation as well as on surface rendering processes.

The idea is to divide the region resulting from "branch merging" into a sub-set of regions in order to allow a one-to-one correspondence between this sub-set and the set of "branches". While the traditional solution to this problem is based on the Voronoi region diagram [7], we propose a more natural morphological *"splitting" approach*.

For simplicity, we consider the situation when two binary, disjoint, and compact objects obj_{11} and obj_{12} in slice 1 merge into one compact object obj_2 in adjacent slice 2. The "splitting" approach is to separate obj_2 into obj_{21} and obj_{22} in order to create an inter-slice one-to-one region correspondence, as shown in Figure 4.

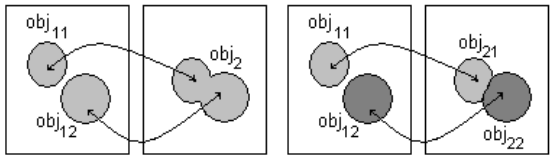

a) b)

Figure 4. Inter-slice region correspondence(see arrows) before (a) and after (b) the region-splitting process

The main steps of our "splitting" approach are :

Step 1. Perform simultaneous and iterative non-conditional dilations on obj_{11} and obj_{12} obtaining $objd_{11}$ and $objd_{12}$ respectively, until $obj_2 \subseteq (objd_{11} \cup objd_{12})$. Since obj_{11} and obj_{12} are disjoint regions, and obj_2 is a compact region, it can be easily proven that $(objd_{11} \cap objd_{12}) \neq \Phi$. The morphological dilation operator is shape preserving, thus $objd_{11}$ and $objd_{12}$ preserve the shape of obj_{11} and obj_{12} respectively.

Step 2. Apply the watershed transform [7] to obj_2 and extract the watershed line *wshl* (i.e. the separation frontier between the regions detected with the watershed transform). As a result of "branch merging", obj_2 preserves to a given extent the shape of both initial "branches", obj_{11} and obj_{12}, thus the watershed transform is to generate the inter-slice one-to-one region correspondence. However, over-segmentation occurs very often when applying the watershed transform.

Step 3. Extract the separation line *sep* that divides obj_2 in obj_{21} and obj_{22} :

$$sep = wshl \cap (objd_{11} \cap objd_{22}) \qquad (8)$$

This step eliminates the over-segmentation effect in the watershed transform. After the minimum number of iterative dilations performed at step 1, the separation limit between obj_{21} and obj_{22} is to be found in the overlapping region of $objd_{11}$ and $objd_{12}$.

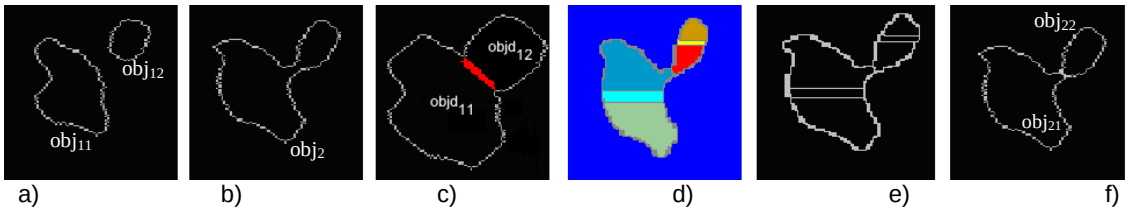

a) b) c) d) e) f)

Figure 5. The "splitting" approach : a) two "branches", obj_{11} and obj_{12}; b) object obj_2 resulting from the "merging" of the two "branches"; c) step 1 : $objd_{11} \cap objd_{22}$ is in red; d) step 2 : over-segmentation of obj_2 in 6 classes (labeled with different colors) with the watershed transform ; e) step 2 : watershed line; f) step 3 : splitting obj_2 into obj_{21} and obj_{22}.

Figure 5 illustrates the main steps in the proposed "splitting" approach. This technique may be easily extended to three or more compact and disjoint "branches" merging into one compact region.

After creating a one-to-one correspondence between regions in adjacent slices, interpolation is performed with the technique described in section 2.1.2. More precisely, this technique generates fixed-length elementary interpolation sequences of intermediate objects simultaneously, for every pair of corresponding regions located in adjacent slices.

2.2. Surface closing

Due to the finite inter-slice distance, the acquisition process rarely provides information about the extremities of the anatomical structures. However, we cannot accept flat-endings in the 3D reconstructed model. To close the surface, we propose a contour-based extrapolation technique which generates a smooth surface closing. First, extreme cross-sections in the sequence of MR shoulder data are to be detected. This detection is based on the maximum inter-slice overlap criterion (8) and on the following definition.

Definition. Given a sequence of saggital slices, region R in slice S(i) is :

a) extreme left if $(\forall)R' \subset S(i-1), C(R,R') = 0$

b) extreme right if $(\forall)R' \subset S(i+1), C(R,R') = 0$

where R' denotes a region in the previous adjacent slice $S(i\text{-}1)$ in *a)* and in the subsequent adjacent slice $S(i\text{-}1)$ in *b)* respectively.

An example of an extreme left region for the scapula is shown in Figure 6.

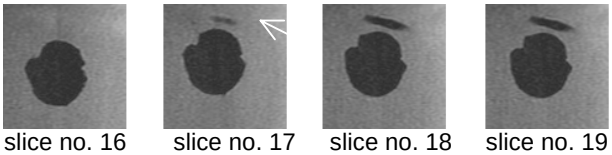

slice no. 16 slice no. 17 slice no. 18 slice no. 19

Figure 6. Sub-sequence of shoulder MR images where the extreme left region of the scapula (white arrow) is detected in slice no.17

We assume that the real extreme saggital slices of the bony structures involved in the articular shoulder complex are one pixel-sized objects, which is a reasonable assumption for this type of structures. To obtain smooth closing, the extreme pixel P is always chosen to be the centre of gravity of the extreme region *obj*. This choice is justified by the fact that all shoulder bones exhibit convex, smooth extremities.

Then, we extrapolate sequences of closing objects located in saggital planes. These sequences are to gradually shrink the extreme region *obj* towards pixel P. The length of a closing sequence is set to (N/2), where N is the even-valued fixed length of the interpolated elementary morphing sequences.

To generate a closing sequence from an initial 2D object and its centre of gravity, the distances from the centre of gravity to each pixel in the object's boundary are computed. We use a 1-D parametric representation for the contour of the object. Therefore, the distances from the centre of gravity to the contour pixels are as follows :

$$DIST(k) = \sqrt{(x - X(k))^2 + (y - Y(k))^2} \qquad k = 1..length(X) \quad (9)$$

where (x, y) are the coordinates of the gravity centre P and [X, Y] is the 1D parametric representation of the contour. These distances are to decrease gradually towards 0 in N/2 iterations. Since the choice of a linear decreasing pattern leads to an angular, disturbing appearance of the extrapolated surface, we propose a non-linear distance decreasing pattern as follows :

$$DIST(k)_i - DIST(k)_{i-1} = i \qquad (\forall)k = 1..length(X) \quad (10)$$

where i is the index of the iteration, i =1..L/2.

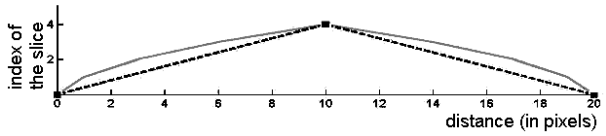

Figure 7. The distance between two symmetric contour points with respect to the centre is decreasing via the non-linear pattern (grey) and via the linear pattern (dashed)

Figure 7 illustrates the difference between the linear decreasing distance pattern and the non-linear decreasing distance pattern specified in (10).

In the end, the extrapolated closing sequences are concatenated at the corresponding extreme regions in the interpolated 3D shoulder model.

2.3. Surface rendering with a triangular mesh

Since the interpolation and extrapolation steps result in a 3-D model where every pair of adjacent slices contain corresponding objects with similar shapes, we propose a new surface rendering technique that exploits this special feature of the reconstructed 3D model. Firstly, we briefly describe how to build a parametric representation of a 2D contour, and secondly we describe the generation of a triangular surface mesh based on the parametric contour representation.

2.3.1. Parameterisation of a 2D contour

We can represent a simple closed contour by figuring a point travelling along this contour and tracing it out.

We need to specify the initial departure position (i.e. the starting pixel) and the travelling direction in the neighbourhood (e.g. clockwise). The travelling point moves from the starting pixel along the contour. Let P(i) be the position of the travelling point at the i^{th} instance of the parameterization process. The next position of the travelling point P(i+1) verifies the following conditions :

a) P(i+1)$\in$ V_8(P(i)), where V_8 is the 8-connectivity neighbourhood, visited in the specified travelling sense.

b) P(i+1)$\notin$ {P(m)| m=1..i}. This condition prevents duplicate elements in the parameterization.

This parameterization approach works well on simple contours with no internal loops, corresponding to compact 2-D regions.

2.3.2. Linking adjacent slices into a triangular surface mesh

Given two adjacent slices in the reconstructed 3D model, we link every pair of corresponding 2D regions with a triangular surface mesh. The map of the inter-slice region correspondence and "branching" is computed before interpolation and updated after extrapolation, since the extrapolation step builds closing sequences corresponding to extreme regions.

Considering two corresponding 2D compact objects located in adjacent slices respectively, we extract and parameterize their contours with the technique described in the section 2.3.1. Next, we generate a triangular surface plot by defining a face matrix. Each row of this face matrix defines a single triangle by indexing into the arrays that contain the coordinates of the vertices.

The generation of triangles between two corresponding contours begins with connecting the starting pixels of the two corresponding 2-D contour parameterizations. Thus, the choice of the starting pixel is not made arbitrarily and the two starting pixels are to share a V_8 neighborhood in a plane orthogonal to the saggital plane.

There are three conditions to be verified in the triangle generation process : a) every triangle has vertices in both corresponding contours; b) the currently generated triangle is of minimal surface; c) considering three successive triangles, the one in the middle does not share the same side with its successor and its predecessor. The triangle generation process is iterative and follows the direction of the contour parameterizations. Supposing that the triangle generated at the kth iteration is (i_1, i_1+1,i_2) then the next generated triangle is the minimal surface triangle between (i_1+1,i_2, i_1+2) and (i_1+1,i_2, i_2+1), where : i_1, i_1+1, and i_1+2 are indexes in the parameterization of the first contour; i_2, i_2+1 are indexes in the parameterization of the second contour respectively (see Figure 8).

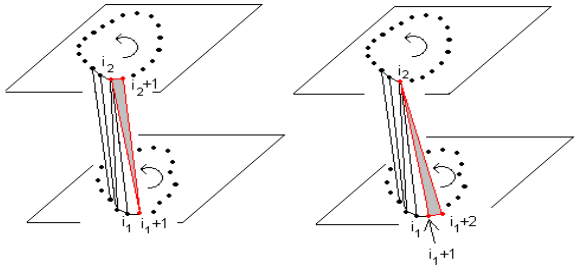

Figure 8. Iterative triangle generation : two options in selecting the minimal surface triangle

The triangle generation process between two corresponding contours stops when every vertex in these contours belongs to at least one triangle.

Considering two adjacent slices, we generate one face matrix for every pair of corresponding objects, then concatenate these matrices into one *inter-slice face matrix*. The concatenation of the object face matrices is accompanied by a correct concatenation of the contour parameterizations into an *inter-slice vertex matrix*. Finally, the face and vertex matrices for the entire 3D model are computed by concatenating all inter-slice and vertex matrices respectively for every pair of adjacent slices.

2.4. Surface fairing

The previously described morphological morphing and surface closing approaches should result into a smooth-surfaced 3D model. However, local irregularities may occur. Some possible reasons for their presence are the shape of the elementary structuring element in the 2D discrete space used in conditional dilation, the elimination of intermediate objects with high-valued redundancy coefficients, and the fixed length of the morphing and closing sequences.

We consider Taubin's surface fairing approach [11] for the linear complexity of the algorithm and for the fact that this approach moves the vertices of the polyhedral surface without changing the connectivity of the faces. Since the faired surface has exactly the same number of vertices and faces as the original one, we can compare the smoothness of the original and of the faired surfaces. We use an alternate definition from [11] for the first order neighbourhood of a vertex : a pair of vertices v_i and v_j are first order-neighbours if they share at least one triangular face in the face matrix of the reconstructed 3D model.

3. Results and geometric evaluation

The geometric validation of the 3D shoulder model does not compare this model to the real shoulder structure, since there is a big gap between the amount of

input information (a sequence of 45 saggital cross-sections) and the amount of output data ($44L+1$ model cross-sections, L=3,5,7). As a consequence of under-sampling, no technique can guarantee to reconstruct the exact anatomy from any set of cross-sections. However, since it contains the input cross-sections at their original locations as specified in the acquisition process, the model is coherent with the input data. Taubin's surface fairing algorithm [11] smoothes the shape of the 2D cross-sections corresponding to the input data, but it performs no shrinking or expanding.

Since the proposed 3D reconstruction approach aims towards a smooth transition between adjacent input shapes and towards a smooth 3D surface closing, we propose a measure of surface smoothness for evaluating the results. For each vertex P, the normal directions to every triangular face containing P are computed, using the classical parametric equations. Among the k normal directions corresponding to P we arbitrarily choose a reference direction (l_0, m_0, n_0), and compute the cosine of the angle between every normal in the set and the reference direction. The average value $\overline{cos\alpha}|_P$ of $cos\alpha_i$, $i=\overline{1,k\text{-}1}$ represents a local measure of smoothness at vertex P. The local smoothness at P increases when $\overline{cos\alpha}|_P$ approaches 1. A global smoothness measure is represented by the histogram of local smoothness measures computed over the entire surface. The histogram of a smooth surface presents a peak value near 1, and low values elsewhere.

The results and evaluation of the reconstructed 3D shoulder model are shown in figure 9. The 3D reconstructed shoulder models shall allow for the precise computation of the minimal distance between the bony structures involved in the shoulder complex during arm rotation.

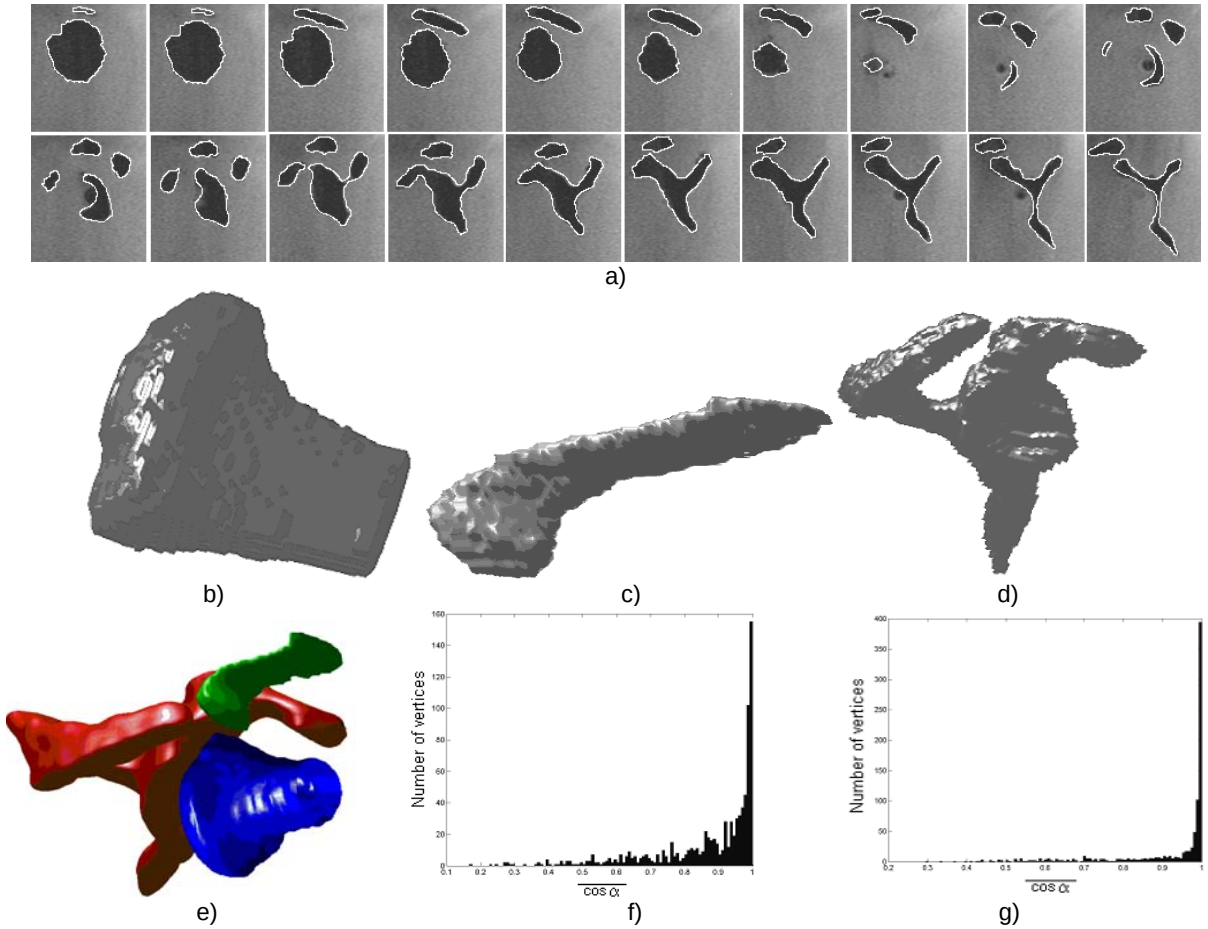

Figure 9. 3-D shoulder model : a) A subset of the input sequence of saggital MR slices for the shoulder reconstruction (the contours of the bony structures are in white); b) reconstructed humerus, unsmoothed; c) reconstructed clavicle, unsmoothed; d) reconstructed scapula, unsmoothed; e) reconstructed shoulder complex, smoothed : humerus is in blue, scapula is in red, while clavicle is in green; f) smoothness histogram for the unsmoothed 3-D shoulder model; g) smoothness histogram for the smoothed 3-D shoulder model

4. Conclusions

In this paper, we propose a new 3D reconstruction technique based on morphological morphing between adjacent slices and on contour-based extrapolation of extreme slices. We believe that the major contribution of our work consists in the proposal of a reconstruction technique based on inter-slice shape similarity that integrates interpolation, extrapolation and surface rendering. The inter-slice shape similarity is a common feature for data in medical imaging when parallel planes are used for the scanning of the anatomic structures. Thus, our approach could be easily extended for the 3-D reconstruction of other types of anatomic structures : soft tissues, blood vessels, brain, etc.

After computing a correspondence map for regions situated in adjacent slices, interpolation is performed with a morphing technique based on conditional dilation. We propose a new approach based on the watershed transform for solving the region "branching" problem. In order to smoothly close the surface of the interpolated 3-D model, we propose a new extrapolation technique.

Surface rendering is based on linking the parametric representations of the 2-D corresponding contours in adjacent cross-sections.

After describing the algorithm we provide experimental results for reconstructing a shoulder model and evaluate these results on a geometric basis.

Thus, we believe that our work represents an important theoretical contribution to the field of 3D imaging, since we propose a new end-to-end reconstruction technique for medical imaging applications. Indeed, our 3D reconstructed shoulder models will soon be used in the study of biomechanics and arthrocinematic of the joint shoulder complex in patients with shoulder pathologies such as instability and impingement.

Future work will concentrate on extending the proposed 3D reconstruction algorithm to other anatomic structures involved in the articular complex of the shoulder (muscles, ligaments, and capsule) in order to pursue the study and analysis of shoulder pathologies.

REFERENCES

[1] W. K. Pratt, *Digital Image Processing*. New York : Wiley, 1991.

[2] S.M. Goldwasser, R.A. Reynolds, D.A. Talton, and E.S. Walsh, "Techniques for the rapid display and manipulation of 3-D biomedical data", *Comput. Med. Imag. Graphics*, vol.12, pp. 1-24, Jan. 1998.

[3] E. H. W. Meijering, "Spline Interpolation in Medical Imaging: Comparison with Other Convolution-Based Approaches", *Signal Processing X: Theories and Applications - Proceedings of EUSIPCO 2000* (10th European Conference on Signal Processing, Tampere, Finland, September 4-8, 2000), vol. IV, 2000, pp. 1989-1996.

[4] S.P. Raya, and J.K. Udupa, "Shape-based interpolation of multidimensional objects", *IEEE Trans. Med. Imag.*, vol.9, pp. 32-42, Mar. 1990.

[5] G.J. Grevera, J.K. Udupa, "An objective comparison of 3-D image interpolation methods", *IEEE Trans. Med. Imag.*, vol. 17, pp. 642-652, Aug.1998.

[6] P.N. Werahera, G.J. Miller, G.D. Taylor, T. Brubaker, F. Daneshgari, and, E.D. Crawford, "A 3-D reconstruction algorithm for interpolation and extrapolation of planar cross sectional data", *IEEE Trans. Med. Imag.*, vol.14, pp. 765-771, Dec. 1995.

[7] J.Serra, *Image Analysis and Mathematical Morphology*. New York : Academic, 1982.

[8] V. Chatzis and I. Pitas, "Interpolation of 3-D binary images based on morphological skeletonization", *IEEE Trans. Med. Imag.*, vol. 19, pp. 699-710, July 1996.

[9] V. Chatzis and I. Pitas, "A generalized fuzzy mathematical morphology and its application in robust 2d and 3d object representation", *IEEE Trans. Image Processing*, vol. 9, pp.1798-1810, Oct. 2000.

[10] A. Bors, L. Kechagias, I. Pitas, "Binary morphological shape-based interpolation applied to 3-D tooth reconstruction", *IEEE Trans. Med. Imag.*, vol.21, pp. 100-108, Feb. 2002.

[11] G.Taubin, "A signal processing approach to fair surface design", Siggraph'95.

[12] A. Branzan-Albu, C. Moisan, and D. Laurendeau, "Tumour detection in MR liver images by integrating edge and region information", Conference on Modelling and Simulation for Computer-aided Medicine and Surgery, MS4CMS'02, Rocquencourt, France, Nov. 2002.